Compact Fiber Optic Sensor for Temperature and Transverse Load Measurement Based on the Parallel Vernier Effect

Tutao Wang, Yaya Mao, Bo Liu, Lilong Zhao, Jianxin Ren, Jiewen Zheng, and Yibin Wan

***Abstract*—An optical fiber sensor based on the parallel Vernier effect for temperature and transverse load measurement is reported in this paper. The sensor is composed of a novel compact fiber Michelson interferometer (MI) and a closed-cavity Fabry–Perot interferometer (FPI) connected in parallel. The fiber MI consists of a bent single-mode fiber (SMF) structure and a short length of hollow core silicon tube (HCST). A section of HCST is fused between two segments of SMF to form the fiber FPI. Two sensors in parallel can easily measure different physical parameters independently, thus realizing multi-parameter sensing. The fiber MI and FPI are used for temperature and transverse load measurement, respectively. Fiber optic MI and FPI are Vernier effect mutual reference interferometers. When MI is used for temperature sensing, FPI is the reference interferometer. When FPI is used for transverse load sensing, MI is the reference interferometer. It can improve the sensitivity of temperature and transverse load. Two samples were made and the sensing experiment was carried out. Through the sensing experiment, we get the maximum temperature sensitivity of 85.1 pm/°C in the temperature range of 30–80 °C and a transverse load sensitivity of −3.15 nm/N in the temperature range of 0–1.96 N. In addition, the sensor has the advantages of tiny size, low cost, and easy manufacture, which is suitable for temperature and transverse load sensing applications.**

***Index Terms*—Fiber optic interferometer sensor, compact structure, parallel Vernier effect.**

I. Introduction

FIBER optic sensors are widely used in mechanical industry, biosensing, structural health and environmental monitoring due to their unique advantages of easy manufacture, anti-electromagnetic interference, and accurate measurement [1], [2], [3], [4]. Optical fiber sensors can be used for measurement of physical parameters, such as temperature [5], refractive index [6], transverse load [7], pressure [8], etc. Temperature and transverse load are important physical parameters in various field.

In recent years, researchers have proposed different types of optical fiber sensors to measure temperature and transverse load, such as the fiber Bragg grating (FBG), long period fiber grating (LPFG), and fiber interferometer sensors [9], [10], [11], [12], [13], [14], [15], [16]. He et al. demonstrated a temperature-insensitive directional transverse load sensor with a measurement sensitivity of 699 pm/(N/mm) based on the FBG, which is located on the section of dual side-hole fiber (DSHF) [9]. Chu et al. conducted an experimental study on temperature and transverse load sensing characteristics of twisted LPFG written by femtosecond laser [10], and the temperature and transverse load sensitivity are 65.31 pm/°C and 4.03 dB/mg. Torres-Gomez et al. proposed a method for simultaneous measurement of transverse load and temperature using LPFGs multiplexed in two wavelength domains with a temperature sensitivity of 50 pm/°C [11]. Compared with fiber grating sensors, fiber interferometer sensors are simpler and cheaper to fabricate. Chen et al. introduced a compact optical fiber tip mode interferometer (FTMI) based on dual wave interference for high temperature and transverse load sensing [12]. The temperature and transverse load sensitivity of the sensor are 14.6 pm/°C and 0.2526 nm/N, respectively. Zhu et al. proposed a hybrid MI and FPI structure-based sensor for high temperature and transverse load sensing and obtained the temperature and transverse load sensitivity of 41.5 pm/°C and 1.09 nm/N [14]. Li et al. designed a fiber optic coaxial Mach–Zehnder interferometer (MZI) with a temperature sensitivity of 45 pm/°C and a transverse load sensitivity of −165 pm/N. MZI is made by fusing a multi-core optical fiber between two short multi-mode optical fibers (MMF) [16].

Among them, reflective optical fiber sensor (FPI and MI) can be used as optical fiber probe, which has very high practical value. Fiber optic FPI is widely used in pressure [8], strain [17], and curvature [18] measurement because of its small size and good stability. Optical fiber FPI is usually insensitive to temperature. The optical fiber FPI used for temperature sensing needs to adopt materials with high thermo-optical coefficients, such as polydimethylsiloxane (PDMS), alcohol and isopropanol, which undoubtedly increases the difficulty and cost of sensor

Manuscript received 7 September 2022; accepted 10 September 2022. Date of publication 13 September 2022; date of current version 27 September 2022. This work was supported in part by the National Key Research and Development Program of China under Grant 2018YFB1800901, in part by the National Natural Science Foundation of China under Grants 62075097, 62075038, 61975084, 61935005, 61835005, 61822507, 62005125, 61875248, 61727817, U2001601, 62035018, 61720106015, and 61935011, in part by the Postgraduate Research & Practice Innovation Program of Jiangsu Province under Grants SJCX22_0346 and KYCX22_1187, and in part by the Jiangsu team of innovation and entrepreneurship, The Startup Foundation for Introducing Talent of NUIST. *(Corresponding author: Yaya Mao.)*

The authors are with the Institute of Optics and Electronics, Jiangsu Key Laboratory for Optoelectronic Detection of Atmosphere and Ocean, Jiangsu International Joint Laboratory on Meterological Photonics and Optoelectronic Detection, Nanjing University of Information Science and Technology, Nanjing 210044, China (e-mail: 1920765116@qq.com; 002807@nuist.edu.cn; bo@nuist.edu.cn; 001967@nuist.edu.cn; 003458@nuist.edu.cn; 403346219@qq.com; 254547694@qq.com).

Digital Object Identifier 10.1109/JPHOT.2022.3206313

manufacturing. Although the fiber MI has good temperature sensitivity, the large size of fiber MI sensors is usually in the centimeter range and cannot meet the sensing applications in narrow spaces. Fiber optic sensors are developing toward miniaturization, and many researchers have proposed fiber MIs with compact size [19], [20], [21]. However, the temperature sensitivity of these sensors is also limited by the reduced size of fiber MI sensors. Therefore, breakthroughs must be made on how to increase sensitivity. The Vernier effect is an effective method to improve the measurement sensitivity. At present, researchers have proposed two mainstream structures to realize the Vernier effect: cascade structure [22] and parallel structure [23], [24]. Compared with cascade structure, parallel structure has been widely studied because of its practical advantages. Paixao et al. demonstrated an optical fiber load sensor, allowing maximum sensitivity values of 0.433 nm/N and 0.66 nm/°C to be attained for vertical load and temperature, respectively [23]. Zhang et al. proposed a highly sensitive bending sensor based on two parallel fiber Michelson interferometers (MIs) with a Vernier-like effect. The experimental results indicate that the bending and temperature sensitivity of the sensor can reach 38.53 nm/m^{-1} and 67.2 pm/°C, respectively [24]. In a parallel structure, two parallel sensors can be manufactured independently during actual manufacturing. In addition, the two sensors in parallel structure are placed in different sensing environments to achieve the multi-parameter sensing.

In this article, a parallel structure consisting of fiber MI and FPI for temperature and transverse load sensing is introduced. Firstly, we designed a novel compact MI sensor, consisting of a bent SMF structure and a short length of HCST. Then, a section of HCST is fused between two segments of SMF to form a closed-cavity fiber FPI and is connected in parallel with the fiber MI. Fiber MI and FPI are used for temperature and transverse load sensing respectively. At the same time, they are mutual reference interferometers. When MI is used for temperature sensing, fiber FPI is the reference interferometer. When FPI is used for transverse load sensing, fiber MI is the reference interferometer. It can improve the sensitivity of temperature and transverse load. Two samples were made for the experiments. The maximum temperature sensitivity is 85.1 pm/°C in the range of 30–80 °C and transverse load sensitivity is −3.15 nm/N in the range of 0–1.96 N. Compared with the condition without the Vernier effect, both the sensitivity of temperature and transverse load is greatly improved.

II. Structure Design and Measurement Principle

Fig. 1(a) shows the structure diagram of the fiber FPI. The length of HCST is D. The light in the fiber core is reflected at the reflective surface M_1 and M_2 of the FPI sensor, resulting in an interference phenomenon. Fig. 1(b) shows the structure diagram of fiber MI. Fiber MI sensor consists of a bent SMF structure and a section of HCST at the end of SMF. The length of the SMF and HCST in the fiber MI sensor is S and L, respectively. α is the bending angle of the SMF. The bent SMF provides an effective excitation and coupling structure for MI sensor. At the same time, the HCST at the end can cause a significant optical path

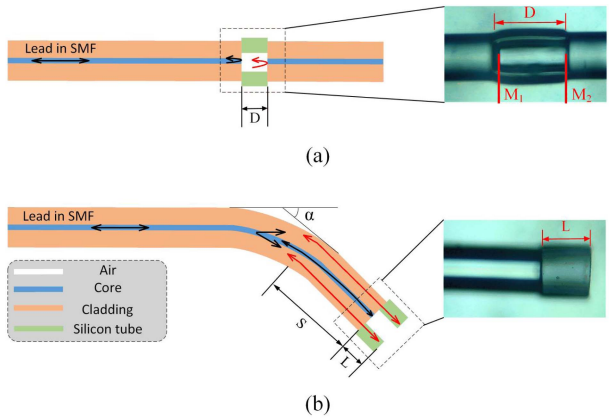

Fig. 1. The schematic diagram of the fiber MI and FPI sensor.

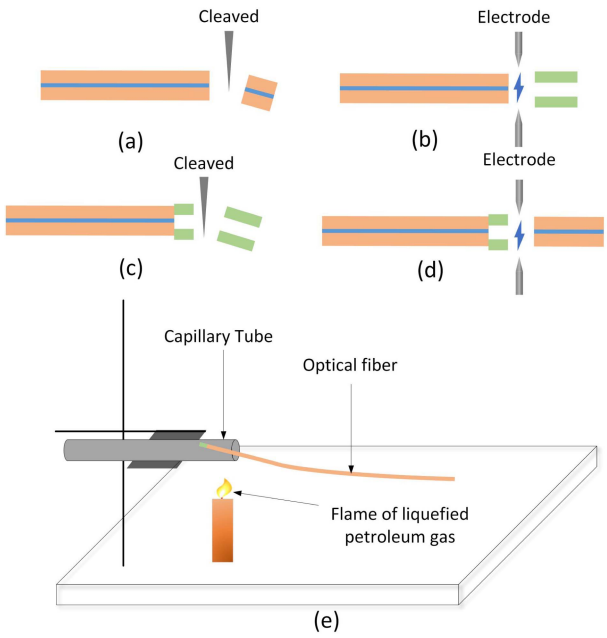

Fig. 2. Schematic of the sensor fabrication process. (a) flat cut the SMF end; (b) fusing the SMF with a section of HCST; (c) flat cut the HCST end; (d) fusing the HCST with a section of SMF; (e) fabrication of the bending structure.

difference between the fiber core and cladding, hence decreasing the size of the MI.

The fabrication process of FPI is shown in Fig. 2(a)–(d). Firstly, we took a piece of bare SMF and used the fiber cleaver to cut its end flat as shown in Fig. 2(a). Then, we used an optical fiber fusion splicer (Fujikura 80s) to splice the SMF with a section of HCST as shown in Fig. 2(b). The discharge intensity of the fusion splicer was set at −25 bit with a discharge time of 300 ms. Next, as shown in Fig. 2(c), the HCST was cut according to the desired length. Finally, the HCST was fused with SMF to form a closed-cavity FPI as shown in Fig. 2(d). The fabrication process of MI is shown in Fig. 2(a)–(c) and (e), which is mainly divided into four steps. The first three steps are the same as the fiber FPI production process. After completing the process in Fig. 2(a)–(c), we inserted the end of HCST into

a silicon tube with an inner diameter of 0.4 mm. The length of the fiber inserted into the silicon tube is S+L. Since the silicon tube has a supporting force to the SMF, the SMF will bend when heated by the flame of liquefied petroleum gas. Different bending angles α can be obtained by adjusting the heating time. The entire manufacturing process does not need to use expensive equipment and materials, only common laboratory materials such as SMF, HCST and some simple processing steps are required.

Fig. 1(a) exhibits the schematic diagram of the fiber FPI sensor. The light in the fiber core is reflected at the reflective surface M_1 and M_2 of the FPI, and the interference effect is generated due to the difference in optical path and refractive index of the two beams. The schematic diagram of fiber MI sensor is shown in Fig. 1(b). Part of the light in the core will leak into the cladding because the light in the fiber core does not satisfy the total reflection condition when propagating to the bending structure. When the light in the cladding propagates to the HCST structure at the MI end, there is a large optical path difference between the light in the cladding and the light in the core. When the reflected light in the cladding returns to the bend structure, it will recouple to the core and interfere with the reflected light in the fiber core. The fiber FPI and MI reflected spectral intensity I_{FPI} and I_{MI} can be expressed as [25]:

$$I_{FPI} = I_1 + I_2 + 2\sqrt{I_1 I_2}\cos\frac{2\pi}{\lambda}\delta_1 \tag{1}$$

$$I_{MI} = I_3 + I_4 + 2\sqrt{I_3 I_4}\cos\frac{2\pi}{\lambda}\delta_2 \tag{2}$$

Where I_1 and I_2 are the reflected light intensities of the reflective surface M_1 and M_2 of fiber FPI. I_3 and I_4 are the light intensity of core mode and cladding modes of the fiber MI, respectively. $\frac{2\pi}{\lambda}\delta_1$ and $\frac{2\pi}{\lambda}\delta_2$ are the phase difference of the FPI and MI. The wavelength of incident light is λ. δ_1 and δ_2 are the optical path difference of the FPI and MI which can be expressed as follow:

$$\delta_1 = 2Dn \tag{3}$$

$$\delta_2 = 2S\left(n_{eff,co} - n_{eff,cl}\right) + 2Ln_{eff,cl} \tag{4}$$

Where D is the length of HCST in fiber FPI and n is the refractive index of air. S and L are the length of SMF and HCST in the fiber MI, respectively. $n_{eff,co}$ and $n_{eff,cl}$ are the effective refractive index of fiber core and cladding, respectively. According to Eqs. (1) and (2), interference dip occurs in the reflection spectrum when phase difference is an odd time of π. Therefore, the wavelength of interference dip can be written as:

$$\lambda_{dip-FPI} = \frac{2\delta_1}{2k+1} \tag{5}$$

$$\lambda_{dip-MI} = \frac{2\delta_2}{2k+1} \tag{6}$$

The free spectral range (FSR) of the fiber FPI and MI can be expressed as:

$$FSR_{FPI} = \lambda_{dip-FPI}(k-1) - \lambda_{dip-FPI}(k) \approx \frac{\lambda^2}{\delta_1} \tag{7}$$

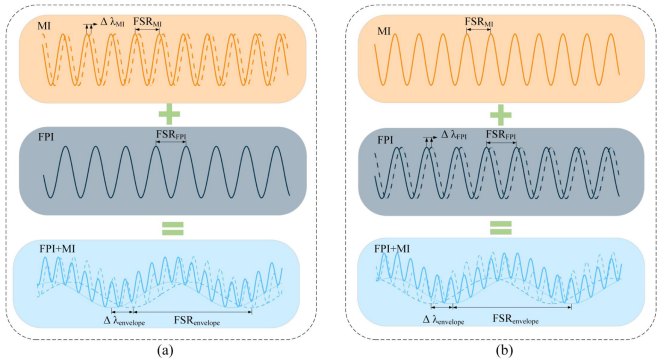

Fig. 3. Schematic diagram of the Vernier envelope shift, the solid and dashed lines indicate the spectra before and after the change, respectively.

$$FSR_{MI} = \lambda_{dip-MI}(k-1) - \lambda_{dip-MI}(k) \approx \frac{\lambda^2}{\delta_2} \tag{8}$$

Thus, the FSR of the Vernier envelope is:

$$FSR_{envelope} = \left|\frac{FSR_{FPI}FSR_{MI}}{FSR_{FPI} - FSR_{MI}}\right| \tag{9}$$

The magnification factor of temperature and transverse load sensing sensitivity are M_T and M_{TL} respectively, which can be expressed as:

$$M_T = \frac{FSR_{FPI}}{|FSR_{FPI} - FSR_{MI}|} \tag{10}$$

$$M_{TL} = \frac{FSR_{MI}}{|FSR_{FPI} - FSR_{MI}|} \tag{11}$$

The schematic diagram of the Vernier envelope shift is illustrated in Fig. 3. Fig. 3(a) and (b) exhibits the effect of MI and FPI spectral wavelength shift on the movement of Vernier envelope, respectively. The reflection spectral wavelength shift of both MI and FPI causes the wavelength shift of the Vernier envelope. The distance of the envelope wavelength shift is a multiple of the wavelength shift distance of the MI and FPI reflection spectra, so the Vernier effect can amplify the sensitivity of the sensor.

In order to investigate the effect of different parameters on the reflection spectra of the fiber optic MI sensor, we experimentally studied the effect of different bending angles on the reflection spectra firstly. The S and L of the fiber optic MI sensor were kept at 2 mm and 200 μm, respectively. We obtained the reflection spectra at different bending angles. The angle was changed from 5° to 25° in steps of 5°. As shown in Fig. 4(a), the extinction ratio (ER) increases and then decreases as the angle increases, because different bending angles change the degree of light leakage from the core to the cladding. The ER is maximum when the bending angle is 15°. Fig. 4(b) shows the fast Fourier transform (FFT) of the spectra at different angles, and it can be found that the spatial frequency is the same.

Through preliminary experiments, we found that the optimum bending angle is about 15°. Then we kept the bending angle at 15° and the size of S at 2 mm. The reflection spectra with different sizes of L are shown in Fig. 5(a), and the spatial frequencies of

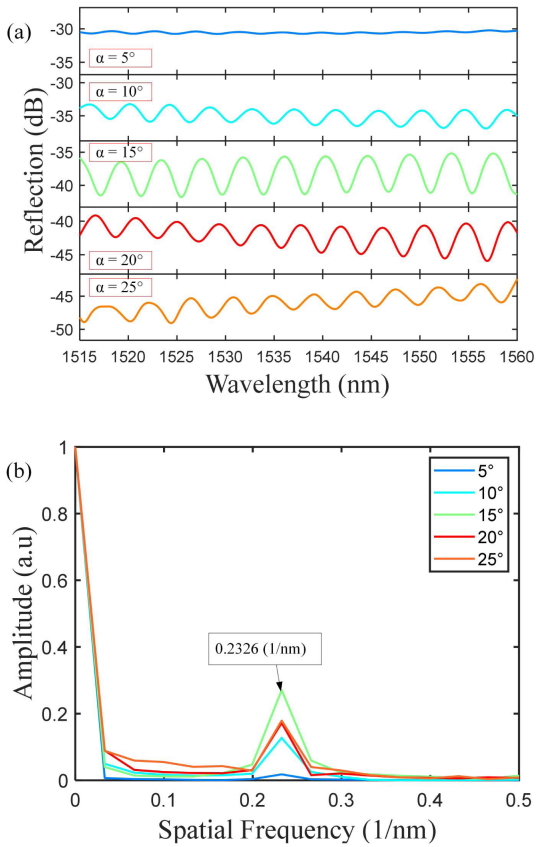

Fig. 4. (a) Reflection spectra at different bending angles; (b) spatial frequency at different bending angles.

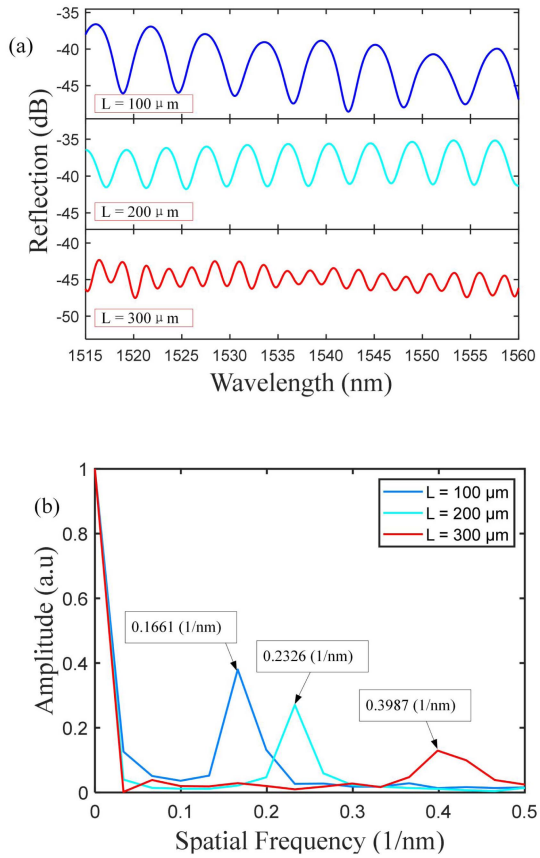

Fig. 5. (a) Reflection spectra with different length of L; (b) spatial frequency with different length of L.

the reflection spectra are shown in Fig. 5(b). The results show that both ER and FSR decrease with the increase of L.

Finally, to investigate the effect of the length S on the fiber MI reflection spectra, we kept the angle at 15° and L at 200 μm. The reflection spectra at different S were obtained by changing the value of S. Fig. 6(a) and (b) show the reflection spectra and the spatial frequency of the reflection spectra at different S, respectively. It can be found that the FSR decreases with the increase of S.

Through the above analysis, two samples were made. The reflection spectra of samples A and B are shown in Figs. 7(a) and 8(a), respectively. In sample A, the value of α is 13°, S is 1.6 mm, and L is 150 μm. The FSR of the optical fiber MI sensor is 6 nm. To generate the Vernier effect, the FSR of the fiber FPI and MI sensor should be close to each other. The cavity length D of FPI in sample A is 200 μm with a FSR of 6.67 nm. Parallel structure-generated envelope has a FSR of 54.4 nm. In sample B, the value of α is 13°, S is 1.6 mm, and L is 120 μm. The FSR of fiber MI sensor is 6.88 nm. The cavity length D of FPI in sample B is 150 μm with a FSR of 7.86 nm. Parallel structure-generated envelope has a FSR of 48.6 nm. Figs. 7(b) and 8(b) show the spatial spectrum of the reflection spectrum, respectively. The spatial frequency of the spectrum generated by the parallel structure includes the spatial spectrum of the optical fiber MI and FPI sensors. Table I records the FSR of MI and

TABLE I
SPECIFIC PARAMETER VALUES OF SAMPLES A AND B

Parameter names	Sample A	Sample B
FSR_{MI}	6 nm	6.88 nm
FSR_{FPI}	6.67 nm	7.86 nm
$FSR_{envelope}$	54.4 nm	48.6 nm
Temperature sensitivity	8.06 pm/°C	8.75 pm/°C
Temperature sensitivity with the Vernier effect	85.1 pm/°C	52.03 pm/°C
Transverse load sensitivity	276.9 pm/N	457.8 pm/N
Transverse load sensitivity with the Vernier effect	-2.3 nm/N	-3.15 nm/N
M_T	10.56	5.95
M_{TL}	8.3	6.88

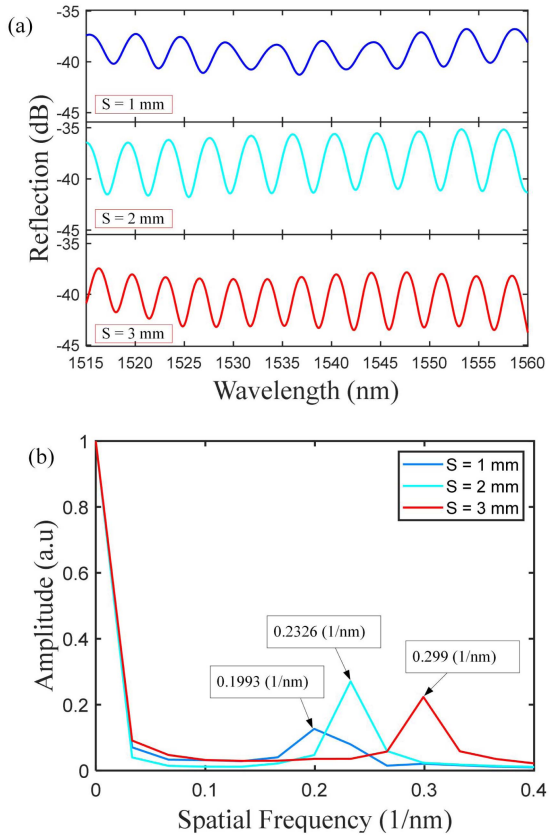

Fig. 6. (a) Reflection spectra with different length of *S*; (b) spatial frequency with different length of *S*.

FPI, temperature and transverse load sensitivity, envelope FSR and the value of magnification factor.

III. Experimental Results And Discussions

The experimental setup for temperature sensing is shown in Fig. 9. The broadband light source (BBS) is used to generate and transmit the optical signal to the fiber optic sensor via a coupler. The optical spectrum analyzer (OSA, Yokogawa, AQ6370D) is used to receive and record the reflection spectra at different temperatures. Fiber MI and FPI are connected in parallel by a 3 dB coupler. The fiber MI is placed in a temperature controller (TC) for temperature sensing experiments, and the fiber FPI is placed at room temperature as a reference sensor.

The temperature sensing experiment was divided into two parts to study the temperature sensing performance without and with the Vernier effect. The temperature was raised from 30 °C to 80 °C in steps of 10 °C by adjusting the TC. Where the TC was adjusted with an accuracy of ±1 °C. The experimental results of temperature sensing for samples A and B are shown in Figs. 10 and 11, respectively. Figs. 10(a) and 11(a) show the reflection spectra of samples A and B without the Vernier effect at different temperatures, respectively. The temperature fitting results of samples A and sample B are shown in Figs. 10(b) and 11(b) with the temperature sensitivities of 8.06 pm/°C and

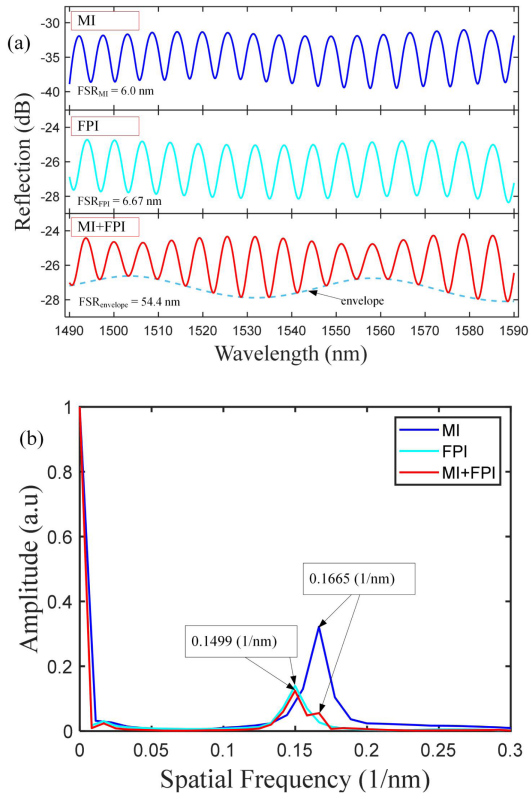

Fig. 7. The reflection spectra and spatial frequency spectra of the fiber MI sensor, the fiber FPI sensor and the parallel structure (sample A).

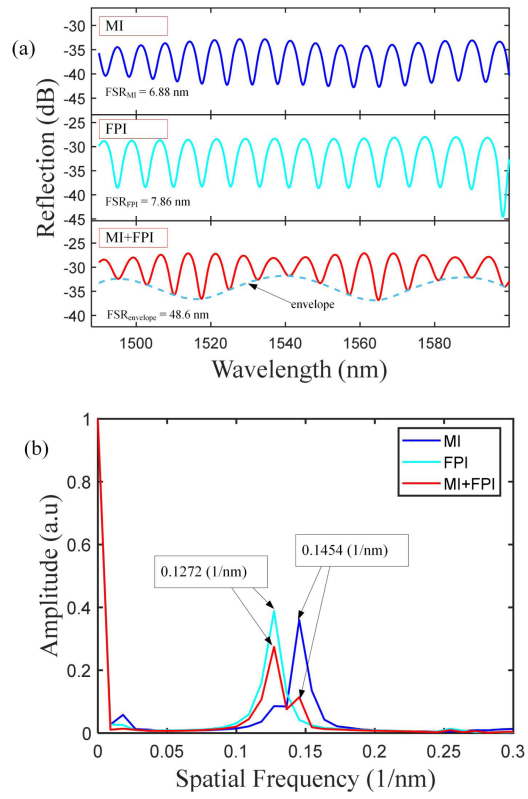

Fig. 8. The reflection spectra and spatial frequency spectra of the fiber MI sensor, the fiber FPI sensor and the parallel structure (sample B).

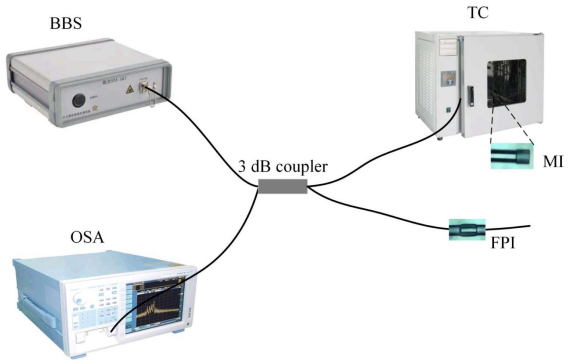

Fig. 9. Schematic diagram of the temperature experimental setup.

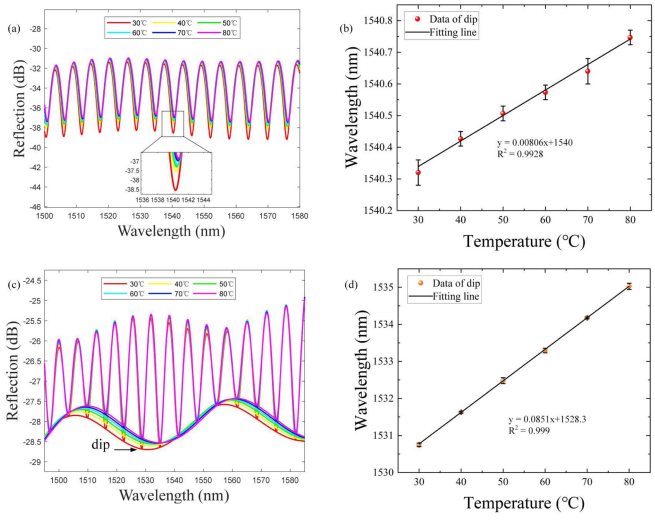

Fig. 10. The temperature sensing experimental results of sample A. (a), (b) the reflection spectra and fitting results at different temperatures without Vernier effect; (c), (d) the reflection spectra and fitting results at different temperatures with Vernier effect.

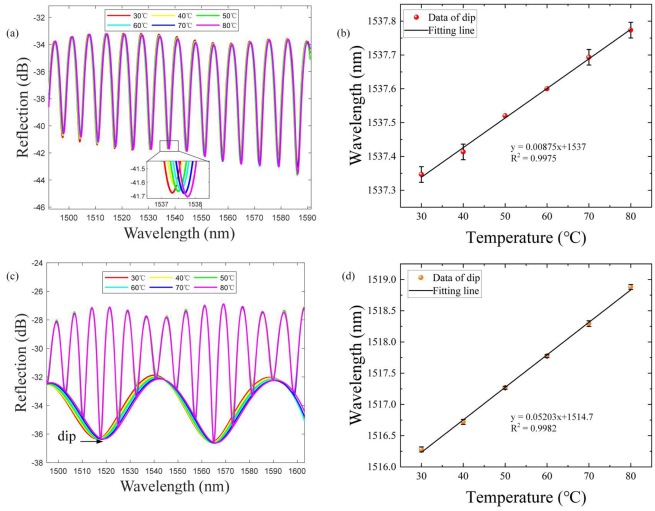

Fig. 11. The temperature sensing experimental results of sample B. (a), (b) the reflection spectra and fitting results at different temperatures without the Vernier effect; (c), (d) the reflection spectra and fitting results at different temperatures with the Vernier effect.

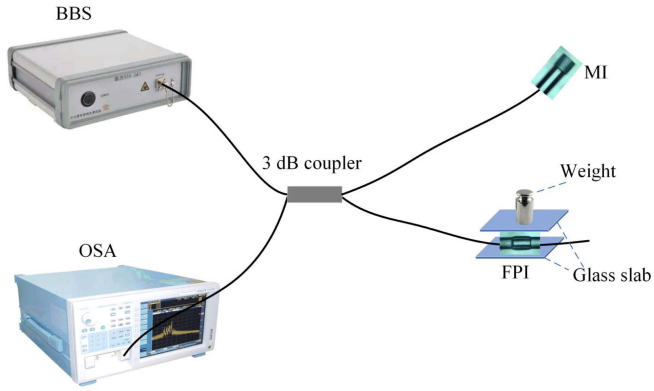

Fig. 12. Schematic diagram of the transverse load experimental setup.

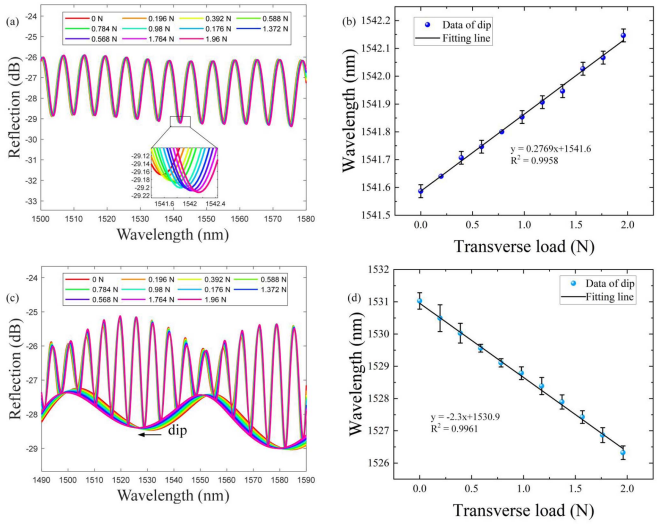

Fig. 13. The transverse load sensing experimental results of sample A. (a), (b) the reflection spectra and fitting results at different transverse loads without the Vernier effect; (c), (d) the reflection spectra and fitting results at different transverse loads with the Vernier effect.

8.75 pm/°C, respectively. Figs. 10(c), (d) and 11(c), (d) show the experimental results of temperature sensing for sample A and B with the Vernier effect. Figs. 10(c) and 11(c) show the reflection spectra of samples A and B at different temperatures. It can be found that with the increase of temperature, the envelope of the reflection spectrum appears red shift. As shown in Figs. 13(d) and 14(d), the maximum temperature sensitivity of samples A and B are 85.1 pm/°C and 52.03 pm/°C, respectively. The magnification factor of sensitivity are 10.56 and 5.95 times, respectively, which is consistent with the calculation result of Eq. (10).

As shown in Fig. 12, the connection method of the transverse load sensing experiment system is the same as the temperature sensing experiment. The difference is that the fiber FPI is used for the transverse load sensor and the fiber MI is used as the reference sensor. In the transverse load experiment, the FPI is placed between two glass slabs. The transverse load is changed by changing the weight on the glass slab.

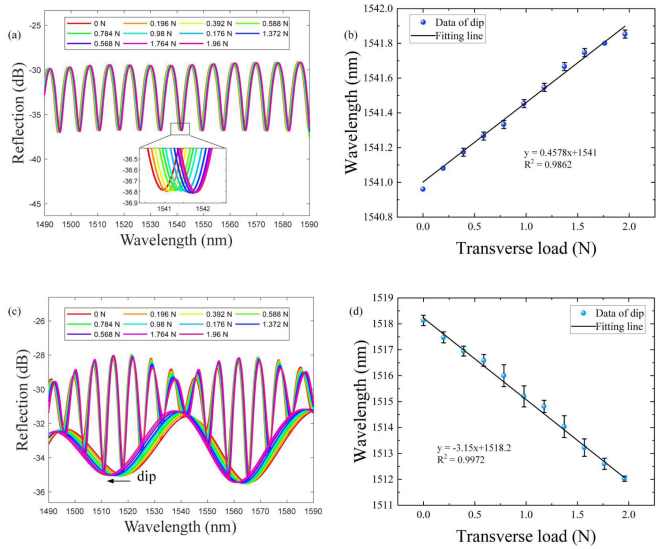

Fig. 14. The transverse load sensing experimental results of sample B. (a), (b) the reflection spectra and fitting results at different transverse loads without the Vernier effect; (c), (d) the reflection spectra and fitting results at different transverse loads with the Vernier effect.

The transverse load sensing experiment was also divided into two parts to investigate the transverse load sensing performance without and with the Vernier effect, respectively. The weight was increased from 0 g to 200 g in steps of 20 g. The reflectance spectra at different weights were recorded by using the OSA. The experimental results of transverse load sensing for samples A and B are shown in Figs. 13 and 14, respectively. Figs. 13(a) and 14(a) show the reflection spectra of samples A and B without the Vernier effect under different transverse loads, respectively. The transverse load fitting results of samples A and B are shown in Figs. 13(b) and 14(b) with the transverse load sensitivity of 276.9 pm/N and 457.8 pm/N, respectively. Experimental results of transverse load sensing with the Vernier effect are shown in Figs. 13(c), (d) and 14(c), (d). Figs. 13(c) and 14(c) show the reflection spectra of samples A and B under different transverse loads. It can be found that with the increase of transverse load, the envelope of the reflection spectrum moves to the side with shorter wavelength. As shown in Figs. 13(d) and 14(d), the maximum transverse load sensitivity of samples A and B are -2.3 nm/N and -3.15 nm/N, respectively. The magnification factor of sensitivity are 8.3 and 6.88 times, respectively. This is consistent with the calculation result of Eq. (11).

We repeated the temperature and transverse load sensing experiments for three times, and added error bars to the sensitivity fitting results. It can be seen that both of the temperature and transverse load experiments have high repeatability of sensor measurement. However, we currently do not have a specific solution for temperature drift to cope with temperature measurements outside the controlled laboratory environment. Therefore, in future research work, FBG or temperature compensation algorithm should be combined with the proposed sensor, so as to solve the problem of temperature drift.

Table II compares the temperature and transverse load sensing performance of the sensor proposed in this paper with other vernier effect-based fiber optic sensors. It can be found that the temperature and transverse load sensitivity of the sensor in this study are at a relatively high level, with a relatively balanced sensing performance. At the same time, it has the advantages of simple fabrication and low cost, and shows a broad prospect in the field of optical fiber temperature and transverse load sensing.

TABLE II
COMPARISON OF SENSING PERFORMANCE WITH REPORTED OPTICAL FIBER SENSORS

Sensor structure	Temperature sensitivity (pm/°C)	Transverse load sensitivity (nm/N)	Ref.
Fiber FPI parallel FPI	27 pm/°C	-	[17]
Fiber FPI cascade FPI	68.9 pm/°C	5.84 nm/N	[22]
Fiber FPI parallel FPI	660 pm/°C	0.433 nm/N	[23]
Fiber MI parallel MI	67.2 pm/°C	-	[24]
Fiber MI parallel FPI	85.1 pm/°C	-3.15 nm/N	This work

IV. CONCLUSION

In summary, a fiber optic sensor for temperature and transverse load measurement based on the parallel Vernier effect is proposed and experimented in this article. The size of the fiber MI sensor can be effectively reduced by splicing a section of HCST at the end of the bent SMF. The Vernier effect is realized by parallel connection of the fiber MI with a traditional closed-cavity FPI. Fiber MI and FPI are used for temperature and transverse load sensing respectively. Through the sensing experiment, we get a maximum temperature sensitivity of 85.1 pm/°C in the temperature range of 30–80 °C and a transverse load sensitivity of -3.15 nm/N in the temperature range of 0–1.96 N. With the advantages of simple fabrication, low cost and tiny size, the proposed sensor has very high practicability and good application prospect.

REFERENCES

[1] V. Budinski and D. Donlagic, "Fiber-optic sensors for measurements of torsion, twist and rotation: A review," *Sensors*, vol. 17, no. 3, 2017, Art. no. 443.
[2] P. Gong et al., "In situ temperature-compensated DNA hybridization detection using a dual-channel optical fiber sensor," *Anal. Chem.*, vol. 93, no. 30, pp. 10561–10567, 2021.
[3] K. Bednarska et al., "Hybrid fiber optic sensor systems in structural health monitoring in aircraft structures," *Materials*, vol. 13, no. 10, 2020, Art. no. 2249.
[4] H.-E. Joe, H. Yun, S.-H. Jo, M. B. G. Jun, and B.-K. Min, "A review on optical fiber sensors for environmental monitoring," *Int. J. Precis. Eng. Manuf.-Green Technol.*, vol. 5, no. 1, pp. 173–191, 2018.

[5] C. Zhu, R. E. Gerald, and J. Huang, "Progress toward sapphire optical fiber sensors for high-temperature applications," *IEEE Trans. Instrum. Meas.*, vol. 69, no. 11, pp. 8639–8655, Nov. 2020.

[6] C. G. Danny, M. Danny Raj, and V. V. R. Sai, "Investigating the refractive index sensitivity of U-bent fiber optic sensors using ray optics," *J. Lightw. Technol.*, vol. 38, no. 6, pp. 1580–1588, Mar. 2020.

[7] J. Zheng et al, "Compact optical fiber sensor based on silica capillary tube for simultaneous high temperature and transverse load measurement," *IEEE Photon. J.*, vol. 14, no. 1, Feb. 2022, Art. no. 6803808.

[8] Y. Zhang et al., "A high precision fiber optic Fabry–Perot pressure sensor based on AB epoxy adhesive film," *Photonics*, vol. 8, no. 12, 2021, Art. no. 581.

[9] J. He et al, "Temperature-insensitive directional transverse load sensor based on dual side-hole fiber Bragg grating," *Opt. Exp.*, vol. 29, no. 12, pp. 17700–17709, 2021.

[10] D. Chu et al., "Temperature and transverse load sensing characteristics of twisted long period fiber gratings fabricated by femtosecond laser," *Opt. Laser Technol.*, vol. 96, pp. 153–157, 2017.

[11] I. Torres-Gómez, A. Martínez-Rios, G. Anzueto-Sánchez, D. E. Ceballos-Herrera, and G. Salceda-Delgado, "Transverse load and temperature sensing using multiplexed long-period fiber gratings," *Photonics*, vol. 8, no. 1, 2020, Art. no. 1.

[12] C. Chen et al., "Compact fiber tip modal interferometer for high-temperature and transverse load measurements," *Opt. Lett.*, vol. 38, no. 17, pp. 3202–3204, 2013.

[13] R. Yang et al., "PDMS-coated S-tapered fiber for highly sensitive measurements of transverse load and temperature," *IEEE Sensors J.*, vol. 15, no. 6, pp. 3429–3435, Jun. 2015.

[14] F. Zhu, Y. Zhang, Y. Qu, H. Su, L. Zhao, and Y. Guo, "Fiber-optic hybrid structure sensor for simultaneous measurement of transverse load and temperature," *Optik*, vol. 208, 2020, Art. no. 164078.

[15] J. Zheng et al., "Simultaneous transverse load, refractive index, and high-temperature sensor based on michelson interferometer," *Opt. Fiber Technol.*, vol. 67, 2021, Art. no. 102686.

[16] Y. Li, Z. Song, J. Wei, and J. Hu, "Fiber in-line Mach-Zehnder interferometer for simultaneous measurement of transverse loading and temperature based on multi-core fiber," *Opt. Laser Technol.*, vol. 143, 2021, Art. no. 107354.

[17] T. Nan et al., "Ultrasensitive strain sensor based on Vernier-effect improved parallel structured fiber-optic Fabry-Perot interferometer," *Opt. Exp.*, vol. 27, no. 12, pp. 17239–17250, 2019.

[18] Z. Bai et al., "Bidirectional bend sensor employing a microfiber-assisted U-shaped Fabry-Perot cavity," *IEEE Photon. J.*, vol. 9, no. 3, Jun. 2017, Art. no. 7103408.

[19] W. C. Wong, C. C. Chan, Y. F. Zhang, and K. C. Leong, "Miniature single-mode fiber refractive index interferometer sensor based on high order cladding mode and core-offset," *IEEE Photon. Technol. Lett.*, vol. 24, no. 5, pp. 359–361, Mar. 2012.

[20] Y. Han et al., "Ultra-compact silicon-microcap based improved Michelson interferometer high-temperature sensor," *Opt. Exp.,* vol. 29, no. 5, pp. 6703–6713, 2021.

[21] L. Duan et al., "Heterogeneous all-solid multicore fiber based multipath Michelson interferometer for high temperature sensing," *Opt. Exp.*, vol. 24, no. 18, pp. 20210–20218, 2016.

[22] Y. Han et al., "High-sensitivity transverse-load and high-temperature sensor based on the cascaded Vernier effect," *Appl. Opt.,* vol. 60, no. 25, pp. 7714–7720, 2021.

[23] T. Paixao, R. Ferreira, M. F. Domingues, and P. Antunes, "Fiber optic load cells with enhanced sensitivity by optical Vernier effect," *Sensors,* vol. 21, no. 22, 2021, Art. no. 7737.

[24] S. Zhang, L. Yin, Y. Zhao, A. Zhou, and L. Yuan, "Bending sensor with parallel fiber Michelson interferometers based on Vernier-like effect," *Opt. Laser Technol.,* vol. 120, 2019, Art. no. 105679.

[25] A. D. Gomes, H. Bartelt, and O. Frazão, "Optical Vernier effect: Recent advances and developments," *Laser Photon. Rev.*, vol. 15, no. 7, 2021, Art. no. 2000588.